Tectonophysics 830 (2022) 229310

Contents lists available at ScienceDirect

Tectonophysics

journal homepage: www.elsevier.com/locate/tecto

The crustal structure of the Cantabrian Mountains revealed by new magnetotelluric soundings

Hoël Seillé [a,b,*], Jaume Pous [a], David Pedreira [c], Jorge Gallastegui [c], Ivan Romero-Ruiz [a], Javier A. Pulgar [c]

[a] Departament de Dinàmica de la Terra i de l'Oceà, Universitat de Barcelona, Barcelona, Spain
[b] CSIRO, Deep Earth Imaging FSP, Australian Resources Research Centre, Kensington, WA, Australia
[c] Departamento de Geología, Universidad de Oviedo, Oviedo, Spain

ARTICLE INFO

Keywords:
Magnetotellurics
Cantabrian Mountains
Subducted Iberian Crust
Hydrated mantle wedge

ABSTRACT

The upper crustal structure of the central Cantabrian Mountains consists of a block of Variscan basement uplifted over the Duero basin as a consequence of a southward displacement along a major thrust during the convergence between Europe and Iberia in the Eocene-Oligocene (Alpine orogeny). We present the results of the 3-D modeling of thirteen new magnetotelluric sites, five of them being completed by long period data, over a 100 km-long, N-S oriented profile across the central Cantabrian Mountains and the Duero basin. Dimensionality analyses indicated a dominant *E*-W direction but with influence of 3-D structures at long periods and locally in the Cantabrian Mountains. Accordingly, we performed a 3-D joint inversion of the full impedance tensor and the geomagnetic transfer function following a sequential inversion workflow. The inverse model presents similarities with existing lithospheric models. In the southern part of the area, the conductive sediments of the Duero basin over a high resistive and homogeneous Iberian lithosphere are well delineated. Towards the north, beneath the Cantabrian Mountains, the model reveals a heterogeneous and conductive lithosphere, in which various elongated and dipping conductors in the upper and middle crust are associated with major Alpine thrusts, one being the frontal thrust of the Cantabrian Mountains over the Duero basin. At deeper depths (between 20 and 35 km depth), the Iberian crust appears as subducting to the north beneath a conductive zone interpreted as the hydrated mantle wedge of the north-Iberian continental margin.

1. Introduction

One of the actions of the Topo-Iberia project (Gallart et al., 2015) was to acquire a number of magnetotelluric (MT) profiles approximately aligned in N-S direction to obtain an integrated transect of the conductivity of the lithosphere across the Iberian plate and Northern Morocco (Anahnah et al., 2011; Pous et al., 2011, 2012; Rodríguez Fernández et al., 2015; Seillé et al., 2015). Here we present the results for the northernmost profile, crossing the central Cantabrian Mountains from the North-Iberian (or Cantabrian) coast to the Duero basin (Fig. 1).

The Cantabrian Mountains, which extend for ~400 km along the northern border of the Iberian Peninsula, constitute the western prolongation of the Pyrenees. To the south, the range is flanked by the Cenozoic Duero foreland basin (Alonso et al., 1996) and, to the north, the contractional deformation that formed the range in the Cenozoic also affected the North-Iberian continental margin and the southern part of the Bay of Biscay abyssal plain (Gallastegui et al., 2002; Pedreira et al., 2015). Three different zones can be differentiated in the Cantabrian Mountains from east to west (Barnolas and Pujalte, 2004): i) the Eastern Cantabrian Mountains, or the Basque-Cantabrian Region, which was formed by the inversion of a thick Mesozoic basin (the Basque-Cantabrian basin) developed in the tip of the Bay of Biscay (e.g. Rat, 1988); ii) the Central Cantabrian Mountains, representing an uplifted block of the pre-Mesozoic basement that holds the higher peaks of the range (Alonso et al., 1996); and iii) the western Cantabrian Mountains, developed also on top of a pre-Mesozoic basement, but with lesser imprint of the Alpine orogeny and lower relief (Martín-González and Heredia, 2011). The MT profile presented in this contribution lies in the eastern border of the central Cantabrian Mountains (Fig. 1a).

The range evolved from different tectonic regimes during the Paleozoic, Mesozoic and Cenozoic. In the Paleozoic, most of the NW Iberian Peninsula constituted part of the continental margin of

* Corresponding author.
E-mail address: hoel.seille@csiro.au (H. Seillé).

https://doi.org/10.1016/j.tecto.2022.229310
Received 2 August 2021; Received in revised form 28 February 2022; Accepted 9 March 2022
Available online 21 March 2022

Gondwana and the collision with Laurussia gave rise to the European Variscan belt, in which the Paleozoic basement of the studied area was part of the foreland fold and thrust belt (Pérez-Estaún et al., 1991). During the Carboniferous-Permian transition, the area was intensely fractured by deep faults that promoted hydrothermal circulation, mineralization and generation of narrow and deep basins (Lepvrier and Martínez-García, 1990; Bastida et al., 2004; Gasparrini et al., 2006; López-Gómez et al., 2019). Faults from this period have a dominant NW-SE trend in the area, although some structures created or reactivated during the Permian have *E*-W to ENE-WSW orientations (Fig. 1).

During the Mesozoic, the area was under an extensional regime related to the opening of the Atlantic Ocean and the Bay of Biscay. The opening of the V-shaped Bay of Biscay and the concomitant counterclockwise rotation of the Iberian Peninsula (Bullard, 1965; van der Voo, 1969) was produced by higher amounts of extension in the western part of the bay than in the east. Undisputed oceanic magnetic anomalies are identified to the west of ~8 °W (e.g. Srivastava et al., 2000: Nirrengarten et al., 2018), while eastwards the extension gave rise to highly stretched continental crust on top of serpentinized mantle beneath the abyssal plain, as far as ~4.25 °W (Ruiz et al., 2017). Even more to the east, the crust is typically continental and the extension focused on several deep basins between Iberia and Europe, locally also exhuming the upper mantle (Vergés and García-Senz, 2001; Jammes et al., 2009; Lagabrielle et al., 2010; Roca et al., 2011; Teixell et al., 2018; Ruiz et al., 2017). One of the larger and deepest basins of the whole Pyrenean-Cantabrian realm was the Basque-Cantabrian basin,

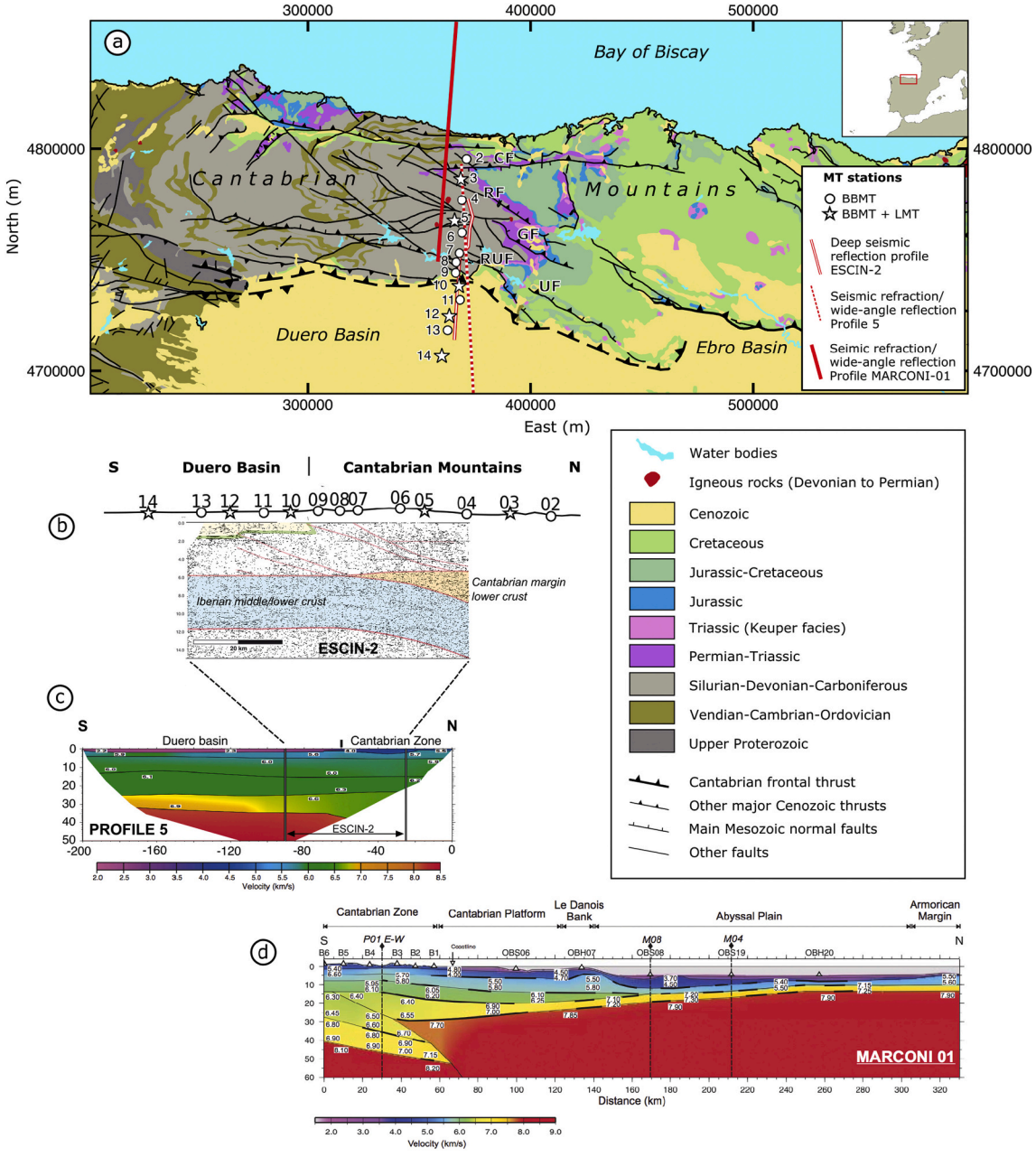

Fig. 1. a) Geological map of the Cantabrian Mountains. White stars are the stations where both broadband (BBMT) and long period (LMT) MT data was acquired. White circles are the BBMT sites. CF, Cabuérniga Fault; GF, Golobar Fault; RF, Rumaceo Fault; RUF, Ruesga Fault; UF, Ubierna Fault. b) Interpreted, coherency filtered stack section of the seismic reflection profile ESCIN-2 (after Pulgar et al., 1996, 1997 and Gallastegui, 2000). c) P-wave velocity model for the seismic refraction/wide-angle reflection Profile 5 (Pulgar et al., 1996; Fernández Viejo, 1997; Gallart et al., 1997). d) P-wave velocity model for the MARCONI-01 seismic refraction/wide-angle reflection profile (Ruiz et al., 2017).

holding near 20 km of sediments on top of an extremely thinned crust (Quintana et al., 2015) and even locally the upper mantle (DeFelipe et al., 2017, 2018). West of the Basque-Cantabrian basin, a thin Mesozoic cover once covered the eroded Paleozoic basement (Fig. 1), being the main Mesozoic depocenter located further north, in the present-day continental platform (Cadenas et al., 2018). A diffuse transfer zone along the Santander and Torrelavega canyons (Pedreira et al., 2007; Roca et al., 2011) separate both depocenters.

Since the Late Cretaceous and during the Paleogene, the plate tectonics setting changed dramatically and the northern drift of the African plate compressed the Iberian subplate against Eurasia, in the context of the Alpine orogeny (Rosenbaum et al., 2002; Macchiavelli et al., 2017). In the Pyrenean realm, this resulted in the underthrusting of the narrow domains of previously exhumed mantle, the inversion of the basins, and the rise of the Pyrenees as a consequence of the continent-continent collision. To the west, the Alpine compressional deformation also affected the North-Iberian passive margin, and the crust beneath the Mesozoic continental platform was uplifted towards the south to form the Cantabrian Mountains (Gallastegui, 2000; Gallastegui et al., 2002, 2016; Pedreira et al., 2015). The erosion of the new reliefs provided the materials that filled the Duero basin over the thin Mesozoic cover (few hundred meters thick) in the Cenozoic (Alonso et al., 1996).

The present-day knowledge of the crustal structure of the Cantabrian has mainly been driven by the seismic experiments carried out in the last decades. The ESCIN-2 deep seismic reflection (Fig. 1b) profile permitted to obtain a detailed image of the lithosphere beneath the Duero basin and the southern part of the Cantabrian Mountains, while several refraction/wide-angle reflection profiles imaged the lithospheric structure also in the northern part of the Cantabrian Mountains and in the Bay of Biscay (Pulgar et al., 1996, 1997; Gallart et al., 1997; Fernández Viejo, 1997; Fernández-Viejo et al., 1998, 2000; Gallastegui, 2000; Gallastegui et al., 2002, 2016; Pedreira et al., 2003). The central part of the Cantabrian Mountains represents a block of Variscan basement uplifted during the Eocene-Oligocene over a deep crustal ramp that is clearly visible in the ESCIN-2 seismic reflection profile (Alonso et al., 1996; Pulgar et al., 1996; Fillon et al., 2016; Gallastegui et al., 2016). The deeper crustal structure is complex, with the development of a double-wedge that includes the subduction of the Iberian crust to the north and the indentation of the Cantabrian Margin crust to the south (Gallastegui, 2000; Pedreira et al., 2003, 2007, 2015; Gallastegui et al., 2016). Gallastegui (2000) and Pedreira et al. (2015) constructed a N-S transect integrating seismic and gravity data that shows the complex imbrication between the Iberian and Cantabrian crusts related to the northward subduction of the middle and lower Iberian crust. This important crustal thickening is accompanied by the deformation of the Cantabrian Mountains, along with several north dipping thrusts that cross the upper crust and converge to a mid-crustal detachment located at 14–15 km depth (Gallastegui, 2000; Gallastegui et al., 2016). However, the inner structure in the thickened area and the maximum depth of the crustal root is still a matter of debate. The ESCIN-2 seismic reflection profile only samples the shallowest part of the root, down to ~42–45 km depth (Gallastegui et al., 2016). On-land seismic stations deployed during the acquisition of the ESCIN-4 marine reflection profile recorded wide-angle reflections produced in a deep and northward inclined discontinuity that can be easily associated with the Iberian Moho, if it continues with the same dipping attitude down to ~53 km depth, at about 15–20 km south of the coastline (Gallart et al., 1997). Similar results were obtained later with the wide-angle records of the marine profiles of the MARCONI project (Fig. 2d; Ruiz et al., 2017) and in a recent reassessment of the seismic data (52 km, Fernández-Viejo et al., 2021). On the other hand, García-Senz et al. (2020) and Teixell (1998), although presenting different models, underline the absence of a negative Bouguer anomaly over the crustal root and limit the maximum depth to ~45 km. However, Pedreira et al. (2015) have shown that a 60 km depth root (or even deeper) is perfectly possible from the isostatic point of view, presenting a petrological-geophysical model that is able to explain not only the Bouguer anomalies, but also the geoid undulations, heat flow, elevation and seismic velocity variations in the mantle.

Along a similar N-S transect, Pous et al. (2001) obtained a 2-D electrical resistivity model using Broad Band Magnetotelluric (BBMT) data. This model revealed north-dipping conductors associated with major Alpine faults, and a deep conductive anomaly located beneath the coastline, which was tentatively interpreted as partial melting of the subducting continental crust, as it was also interpreted further to the east in the Pyrenees (Pous et al., 1995a, 1995b; Ledo et al., 2000; Campanyà et al., 2011).

The new MT profile we present in this contribution was acquired approximately along the line of the ESCIN-2 seismic reflection profile (Fig. 1a; Pulgar et al., 1996; Gallastegui et al., 2016), which was also the line followed by the old BBMT profile (Pous et al., 2001). The new MT data have a high coverage of MT stations in the Cantabrian Mountains and record long-period data, which reach deeper levels of the lithosphere. We derive a 3-D resistivity image using the full impedance tensor and vertical transfer functions, to obtain a reliable and accurate image of

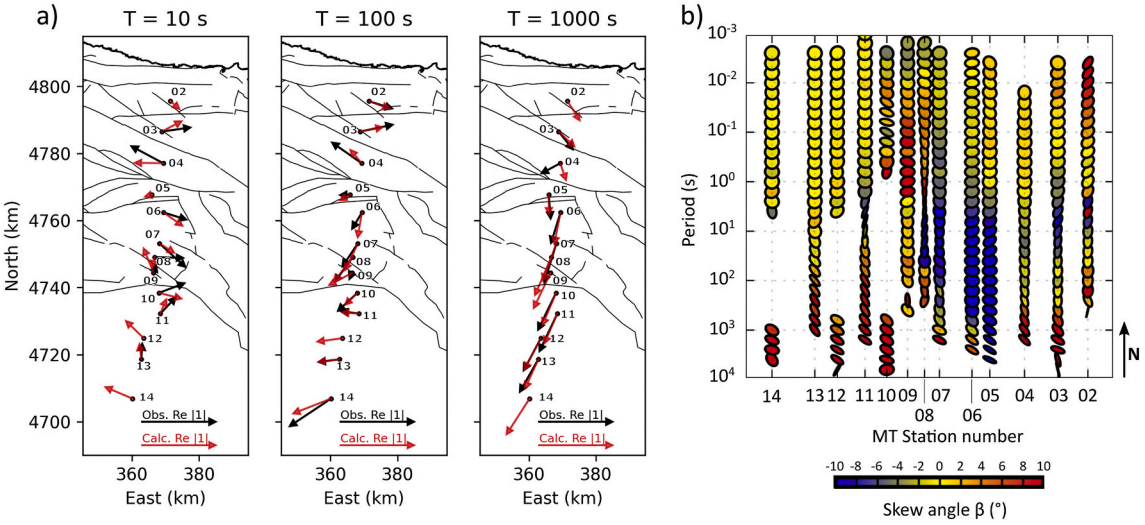

Fig. 2. a) Real induction arrows for three periods, in Wiese convention (pointing away from conductors). In black: the observed real induction arrows, in red: the responses of the 3-D model shown in Fig. 6 and Fig. 7. b) Phase tensor ellipses of the observed data filled with the skew angle β. The ellipses are oriented with the North pointing to the top of the plot. (For interpretation of the references to color in this figure legend, the reader is referred to the web version of this article.)

the crustal structure of this orogen. The 3-D model is interpreted jointly with the available geophysical and geological data in order to achieve a deeper understanding of the crustal structure and the geodynamic history of this area.

2. New MT data

The magnetotelluric method (MT) is a passive electromagnetic method that uses the natural variations of the electric and magnetic fields to infer the distribution of electrical conductivities within the subsurface. The horizontal magnetic **H** and induced electric fields **E** are related in the frequency domain by the complex impedance tensor **Z**. In a similar way, the horizontal and the vertical components of the magnetic field are related by a complex vector, the vertical field transfer functions (VTF). Distortion of the electric and magnetic fields by heterogeneities present in the near-surface affects more the impedance tensor Z than the VTF and, when used in conjunction, the reliability of the geoelectrical models can be improved (Berdichevsky et al., 2003). In this study both the impedance tensor Z and the VTF are modelled jointly.

The new long period magnetotelluric profile crosses the central Cantabrian Mountains and the northern part of the Duero foreland basin (Fig. 1). The data consist of thirteen magnetotelluric sites over a N-S, 100 km long profile. The five components of the electromagnetic field were recorded in N-S and E-W directions. Six MT sites (marked as stars in Fig. 1) were recorded using both broadband (BBMT) and long period (LMT) instruments, allowing us to obtain MT transfer functions with periods ranging from 0,001 s to 10,000 s. Seven sites were acquired using BBMT instruments only (marked as circles in Fig. 1), obtaining transfer functions with periods ranging from 0,001 s to 2000s. Space between sites varies between 5 and 10 km. The BBMT data were processed using the robust bounded influence remote reference processing (BIRRP) algorithm (Chave et al., 1987), while the LMT data were processed with the algorithm of Varentsov (2006).

Fig. 2a shows the VTFs data in the form of induction arrows (real part) for three periods in the Wiese convention (pointing away from conductive zones). The vectors magnitude does not exceed values of 0.5, even the ones located close to the coast. A general NNE-SSW orientation can be observed at long periods ($T = 1000$ s) while at shorter periods (T = 10 s) the vectors point perpendicularly to the profile, especially in the northern part of the profile, between sites 02 and 08. The effect of the seawater of the Bay of Biscay was tested through forward modeling. A conductor of 0.33 Ωm following the bathymetry was embedded in a homogeneous half space of 100 Ωm. The real part of the induction arrows of such model point to the south with smaller magnitudes compared to the observed arrows. We concluded that the behavior of the observed induction arrows can only be explained by some three dimensional or off-profile structures located on land.

The XY component shows phases greater than 90° above 100 s for sites 06 and 07, and above 1000s for site 05 (Supporting Information Fig. S1). These anomalous phases are accompanied with a strong decay in the apparent resistivity towards extremely conductive values ($\rho_{app} < 1$ Ωm). This type of anomalous phases accompanied by a drop in the apparent resistivity was observed in several geological settings, where different physical or geological causes were invoked: electrical anisotropy (e.g. Heise and Pous, 2003), current channeling (Lezaeta and Haak, 2003), 3-D conductive bodies such as ring conductors (Weckmann et al., 2003a, 2003b) or L-shape bodies (Ichihara and Mogi, 2009). No evidence of electrical anisotropy can be inferred from local geology in the Cantabrian Mountains. The location of sites 05, 06 and 07, close to a complex intersecting pattern of WSW-ENE and NW-SE oriented faults (Fig. 1), suggests that the effect on the electromagnetic fields causing phases exceeding 90° is probably due to a complex-shaped conductor, which could be assimilated to an L-shape.

3. Magnetotelluric data analysis

Directionality and dimensionality information of the geoelectrical structures of the subsurface can be extracted from the analysis of the impedance tensor Z. The conclusions of such analysis can be used to get a general understanding of the subsurface conductivity distribution but also to justify the approach that will be used to model the MT data.

Caldwell et al. (2004) introduced the phase tensor, which is defined as the ratio of the imaginary and real parts of the impedance tensor **Z**. This tensor is unaffected by galvanic distortion and can be represented graphically as an ellipse, which principal axes orientation indicates directions of resistivity gradients. Fig. 2b shows the phase tensor ellipses of the observed data. The color used to fill the ellipses is the phase tensor skew angle|β|, which defines the asymmetry of the phase tensor and indicates the presence of 3-D effects (Caldwell et al., 2004). For periods lower than 1 s, the ellipses show a relative 1-D behavior for most of the sites, with circularly shaped ellipses and $|\beta| < 4°$. Above 100 s, $|\beta| > 4°$ for most of the sites. At periods ranging from 100 s to 10,000 s, the major axis of the ellipses is oriented along WNW-ESE and NW-SE directions, and $|\beta| > 8°$, clearly indicating a 3-D structure at long periods. Sites 05, 06 and 07 with phases greater than 90° have a high skew angle ($|\beta| > 6°$) from 10 s to longer periods.

Dimensionality was also assessed using the multisite/multiperiod analysis (McNeice and Jones, 2001) based on the Groom and Bailey (1989) impedance tensor decomposition. For this analysis, data with a 3-D behavior was not considered ($T > 300$ s). Assuming an error floor of 8%, a strike direction of N100°E was obtained between 0.1 s and 300 s for all the sites.

Same observations were made applying the method of Bahr (Bahr, 1988). A dominant strike direction could be estimated between N90°-100°E. The estimation of data affected by 3-D effects using the Bahr phase sensitive skew is coherent with the phase tensor analysis.

The induction arrows and the three distinct approaches used for estimating the dimensionality and directionality of the MT data (the phase tensor, the Bahr method and the Groom and Bailey method) gave similar results. They point to a regional 2-D structure oriented ~N100°E with 3-D effects at long periods (longer than 300 s) for all the sites along the profile, and strong localized 3-D effects at intermediate periods for several MT sites localized within the Cantabrian Mountains. Consequently, we decided that a 3-D approach would be more suitable for this dataset.

4. Three-dimensional inversion

The 3-D inversion was carried out using the 3-D inversion algorithm WSINV3DMT developed by Siripunvaraporn and Egbert (2009). This code allows to carry out the joint inversion of the impedance tensor Z and the vertical transfer functions (VTF). The algorithm minimizes an objective function comprised by a misfit term and a model term, in order to obtain a minimum structure model that fits the data to a certain target misfit.

The starting resistivity model is a uniform 100 Ωm half space, which includes the sediments of the Duero basin (modelled as a 10 Ωm feature), inferred from seismic and geological studies (Heredia et al., 2010). It was left as a free parameter during the inversion. The Atlantic Ocean to the north was also included following the bathymetry (ETOPO1, Amante and Eakins, 2009). The seawater resistivity was set to 0.33 Ωm and it was kept fixed during the inversion. Since the aim of this study is to investigate the deep structure, topography was not included in the inversion.

Model grid dimensions were 32 × 66 × 60 cells in the X (North), Y (East) and Z direction respectively. Vertically, we define the first layer being 30 m thick, increasing logarithmically at depth. Horizontally, in the core of the model the cells have dimensions of 1.75 km × 1.75 km. The padding of the model has cell sizes that are increasing logarithmically in both directions to a sufficient extent to satisfy the boundary

conditions of the forward solver.

The thirteen sites were used for the inversion, with 12 periods between 0.25 s and 6309 s. Both the impedance tensor and the VTF were included in the inversion. An error floor of 5% of the geometric mean of the off-diagonal components of the impedance tensor ($0.05 \times \sqrt{Z_{xy}Z_{yx}}$) and 15% for the vertical transfer functions ($0.15 \times \sqrt{|T_{zx}|^2 + |T_{zy}|^2}$) was applied.

4.1. Inversion strategy

3-D inversion of a unique MT profile is not only sensitive to the resistivity distribution beneath the profile but also to off-profile structures (Siripunvaraporn et al., 2005; Patro and Egbert, 2011; Brasse et al., 2015). However, it is exposed to greater ambiguity away from the MT sites. In order to prevent problems that might arise from full 3-D inversion (Z and VTF) on profile data, e.g. significant off-profile resistivity structures (Siripunvaraporn et al., 2005), we adopted a sequential inversion strategy that allowed to fit the full data while keeping reasonably smooth structures across strike (off profile), as expected for this dataset, which is moderately affected by 3-D effects. The strategy consisted in: 1] Inversion of the off-diagonal components of the impedance tensor, excluding the phases higher than 90°. 2] The inversion was restarted adding the VTF data. 3] The inversion was restarted including the diagonal components of the impedance tensor, along with the off-diagonal terms with phases higher than 90°. The models obtained at the end of each step are shown in Fig. 3.

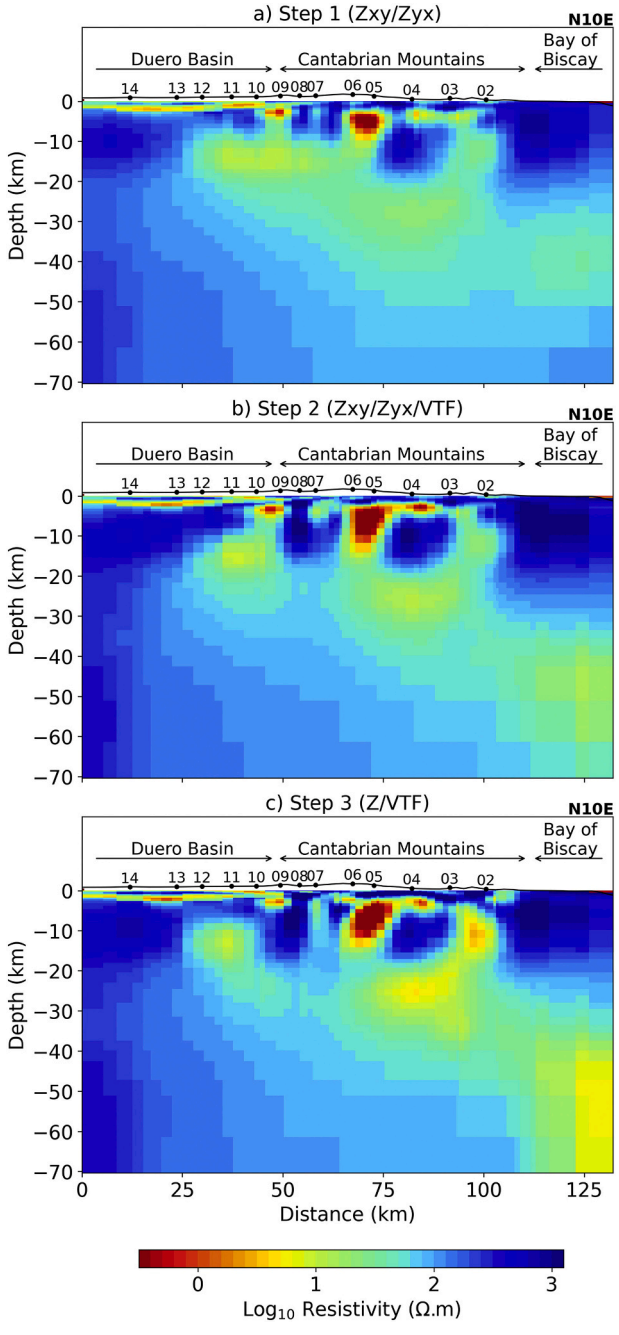

Fig. 3. N10°E oriented cross section across the 3-D resistivity volumes for a) Step 1: inversion of Zxy/Zyx impedance data, b) Step 2: restarting from Step 1, inversion of Zxy/Zyx/VTF data and c) Step 3: restarting from Step2: inversion of the full Z/VTF data.

The advantage of this strategy over an inversion using the complete dataset at once is the reduction of off-profile artefacts. Because the diagonal components of the impedance tensor are strongly affected by off-profile structures, this strategy allowed obtaining a model that was primarily driven by the off-diagonal terms of the impedance tensor. We observed that the main structures constituting the final model were already present at the end of the first inversion step including only the off-diagonal elements of the impedance tensor (Fig. 3a). The VTF data are more sensitive to horizontal resistivity contrasts than to depths or absolute values of resistivity (Siripunvaraporn and Egbert, 2009). Adding it at a later stage kept the shape of the structures and mainly enhanced or reduced these contrasts (Fig. 3b). The fitting of the phases greater than 90° and the diagonal elements of the impedance tensor was achieved in the last step of the inversion (Fig. 3c).

This strategy was found to be optimum for the inversion of this dataset and the 3-D model obtained is in agreement with previous studies (deep seismic reflection profile – Pulgar et al., 1996, and seismically-constrained gravity models - Gallastegui, 2000; Pedreira et al., 2015; Gallastegui et al., 2016).

The inversion was run on a Linux operating system with a machine of 128 GB Ram. Each iteration lasted about 4 h. The inversion process reached a final normalized root mean square (RMS) of 1.8 after a total of 17 iterations. The fitting of the full Z and the VTF is satisfactory taking into account the error floor used. Fig. 4 shows the fitting of apparent resistivity, phase and VTFs for four selected sites. The complete dataset and model responses can be found in the Supplementary Information 1.

The RMS by components (grouped by Z and VTF), by site and by period is shown in Fig. 5. Most MT sites present low RMS values across the complete period range. However, there is an underfit of some of the VTF data at high frequencies.

4.2. 3-D model

The 3-D inverse model is presented in Fig. 6 and Fig. 7. Fig. 6 shows three N-S sections and a cross-section oriented N10°E across the 3-D volume. The N10°E cross section presents the model located directly under the MT sites, coinciding with the direction of the MT profile, it was chosen for the interpretation. Fig. 7 shows horizontal slices at several depths. The main features are labelled in Fig. 6d and Fig. 7.

The model presents minor variations in the E-W direction perpendicular to the profile. Most of the off-profile variations occur in the upper part of the model (above 15 km depth) within the Cantabrian Mountains.

A shallow subhorizontal conductor C1 (2–30 Ωm) is located in the southern part of the profile (Fig. 6d). It is 2 to 2.5 km thick beneath sites 10 to 12 and gets thicker to the south, up to 3.5 km beneath site 13. This conductor, which corresponds to the Cenozoic sediments of the Duero basin, was already present in the starting model. However, the inversion modified its geometry under sites 13 and 14, extending the conductor deeper, up to 3.5 km.

Several shallow conductors (1–20 Ωm) appear in the Cantabrian Mountains (Fig. 6d). Most of them are subvertical to north dipping and

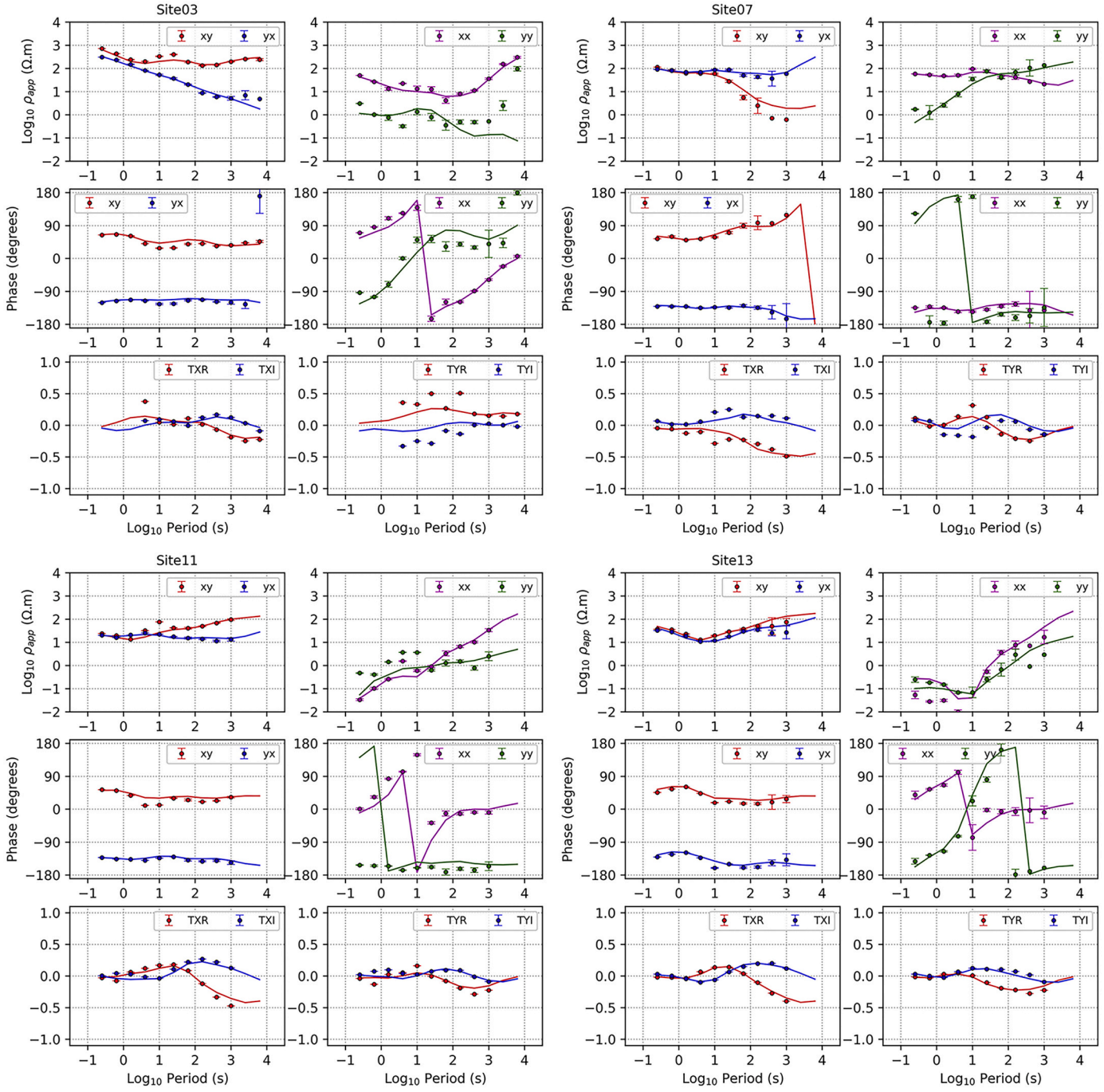

Fig. 4. Data (points) and responses of the 3-D inverse model (continuous line) at four selected sites (03 / 07 / 11 / 13).

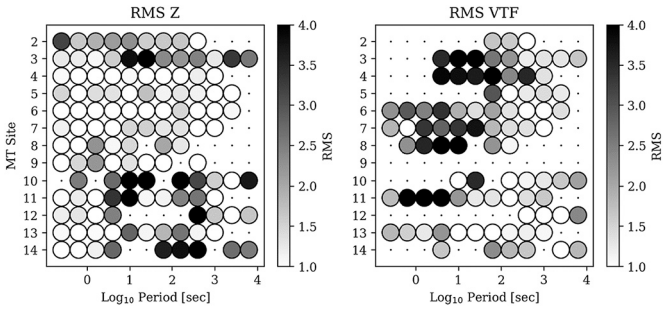

Fig. 5. RMS values at all sites and all frequencies for the impedance tensor Z (left) and the vertical transfer function (right).

extend from the surface to 5–10 km depth. The orientation varies from E-W to NW-SE (Fig. 7). Conductor labelled C2a is located at the transition between the Duero basin and the Cantabrian Mountains, and is linked to the conductor C1. Conductor C2b appears to be dipping south (Fig. 6c and Fig. 6d) and extend to a depth of 10 km. It is mainly E-W oriented (Fig. 7). Conductor labelled C2c is located in the northern part of the model and reaches a maximum depth of 15 km, its connection to conductor C4 is unclear.

Conductor C3 (~ 10 Ωm) appears beneath the northern border of the Duero basin (sites 11 and 10) at depths between 10 km to more than 25 km. This conductor presents a north dipping behavior on the eastern side of the profile (Plane X18, Fig. 6c). At more than 20 km depth it shows a roughly N-S orientation, following the orientation of the MT profile (Fig. 7). On the western site this conductor is local and reaches ~15 km

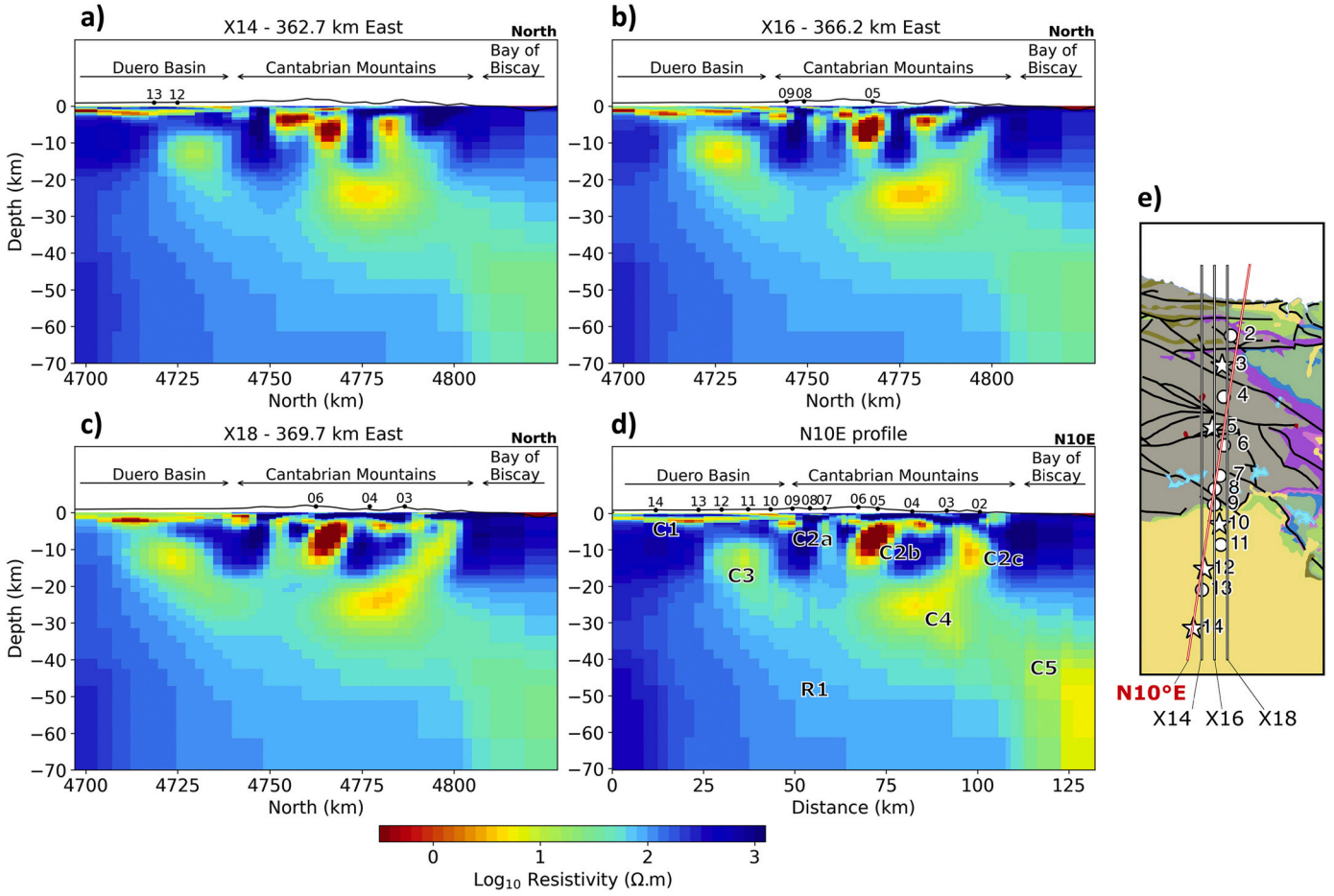

Fig. 6. Vertical slices through the 3-D inverse model. a), b) and c) N-S oriented planes of the core area of the model: planes X14, X16 and X18, respectively. MT sites directly located above the N-S section are indicated. Each plane is separated 3.5 km from each other. d) N10°E oriented cross section across the 3-D resistivity volume. e) Geological map with the location of the profiles.

depth.

The conductor C4 (5–30 Ωm) is located between 20 and 30 km depth beneath sites 04 to 03 and is subhorizontal (Fig. 6d). It appears to extend deeper until 35 km depth in the northern part of the model under site 03. At 25 km depth (Fig. 7) its lateral continuation has roughly an E-W orientation.

Conductor C5 (20–50 Ωm) is located 15 km north of site 02, outside of the site coverage and reaches depths of more than 70 km. Sensitivity tests (see below) indicate that this structure is not well constrained.

Below the conductive zones the model shows a resistor R1 with resistivities higher than 100 Ωm in the subducting slab and up to several 1000's of Ωm beneath the Duero basin in the southern part of the profile. Its top is dipping northwards (Fig. 6) and it appears to be E-W oriented at all depths (Fig. 7). The location of the top of this resistive body is coherent with the seismic signature of the top of the lithospheric mantle beneath the Iberian crust. Subducting slabs have been modelled as dipping resistors in several studies using MT (e.g. Matsuno et al., 2010; Evans et al., 2014; McGary et al., 2014; Heise et al., 2019), with values ranging from 500 Ωm (Heise et al., 2019) up to 10.000 Ωm (Evans et al., 2014). In their study, Matsuno et al. (2010) pointed out the low sensitivity of the MT data to the resistive slab, due to the low sensitivity of the MT method to resistors beneath thick conductors (e.g. Chave and Jones, 2012). In the case of the Cantabrian Mountains, the subduction is less pronounced and relatively shallow compared to active and deep subduction zones. The subcontinental lithospheric mantle is assumed to be essentially anhydrous (Evans, 2012), explaining its high electrical resistivity, which generally contrasts with the hydrated nature of the mantle wedge, which tends to present higher electrical conductivities. Our final 3-D model agrees with a subducting resistive mantle, especially when the top of R1 dips northwards.

4.3. Model assessment

Non-linear sensitivity tests were performed to determine if the presence of the geoelectrical structures observed in the model are required by the data. These tests consist in perturbing part of the preferred model, compute its response and compare it with the responses of the preferred model. To assess how significantly responses differ from one to another we use an *RMS update*, as previously introduced by Garcia et al. (2015). The *RMS update* is defined as:

$$RMS\ update(\%) = 100 \times \frac{RMS - RMS_0}{RMS_0}$$

RMS_0 corresponds to the final inverse model and RMS to the perturbed model. The RMS is defined as:

$$RMS = \sqrt{\frac{1}{N}\sum_{i=1}^{N}\frac{(d_i - f_i)^2}{\varepsilon_i^2}}$$

where d_i is the observed data, f_i are the model responses and ε_i the data error. The RMS is normalized by the number of observed data points N. An RMS value of 1 indicates that the misfit term is equal to its estimated error, or in other terms, that the data is perfectly fitted within its error. Because the RMS is calculated using the data errors after applying the

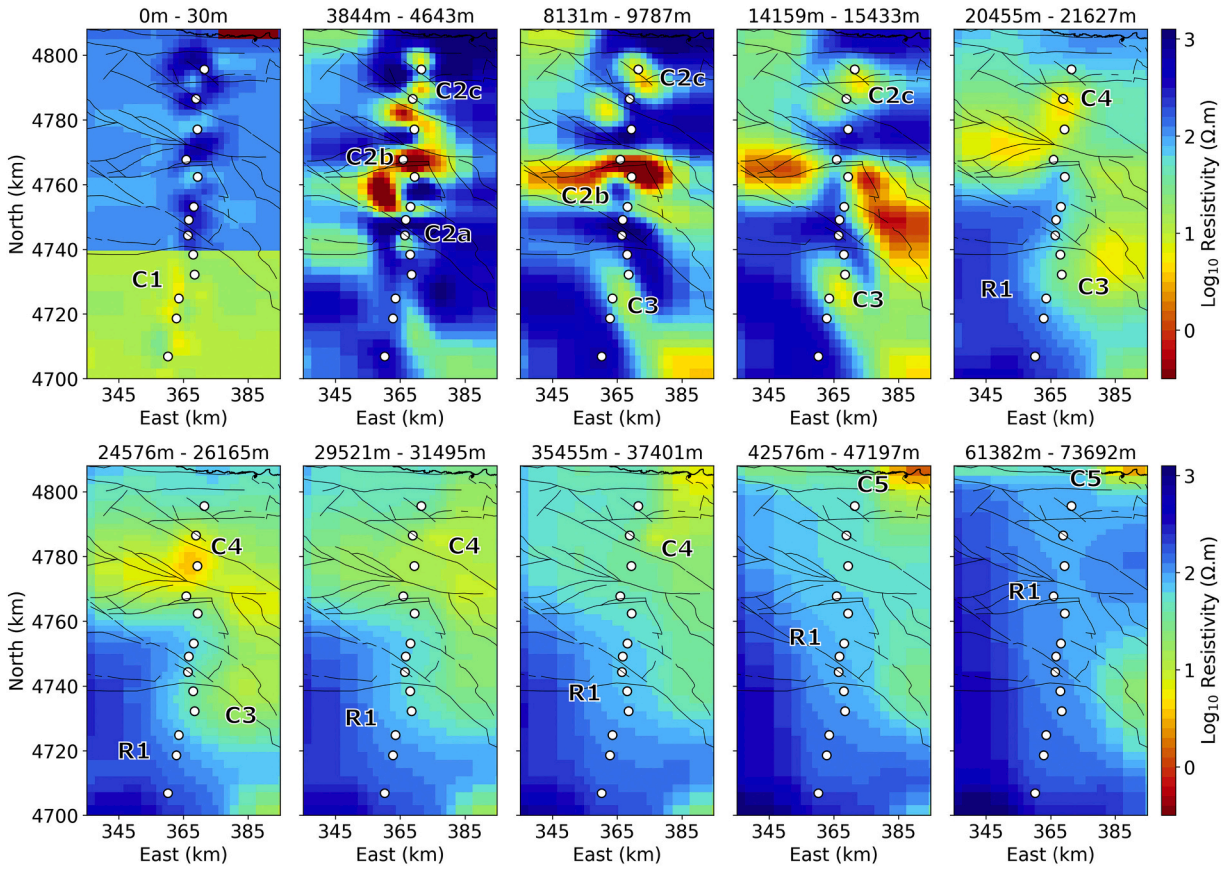

Fig. 7. Horizontal slices through the 3-D inverse model at several depths. MT sites are marked as white circles. Thin black lines are the main faults in the area. The model features are described in the text.

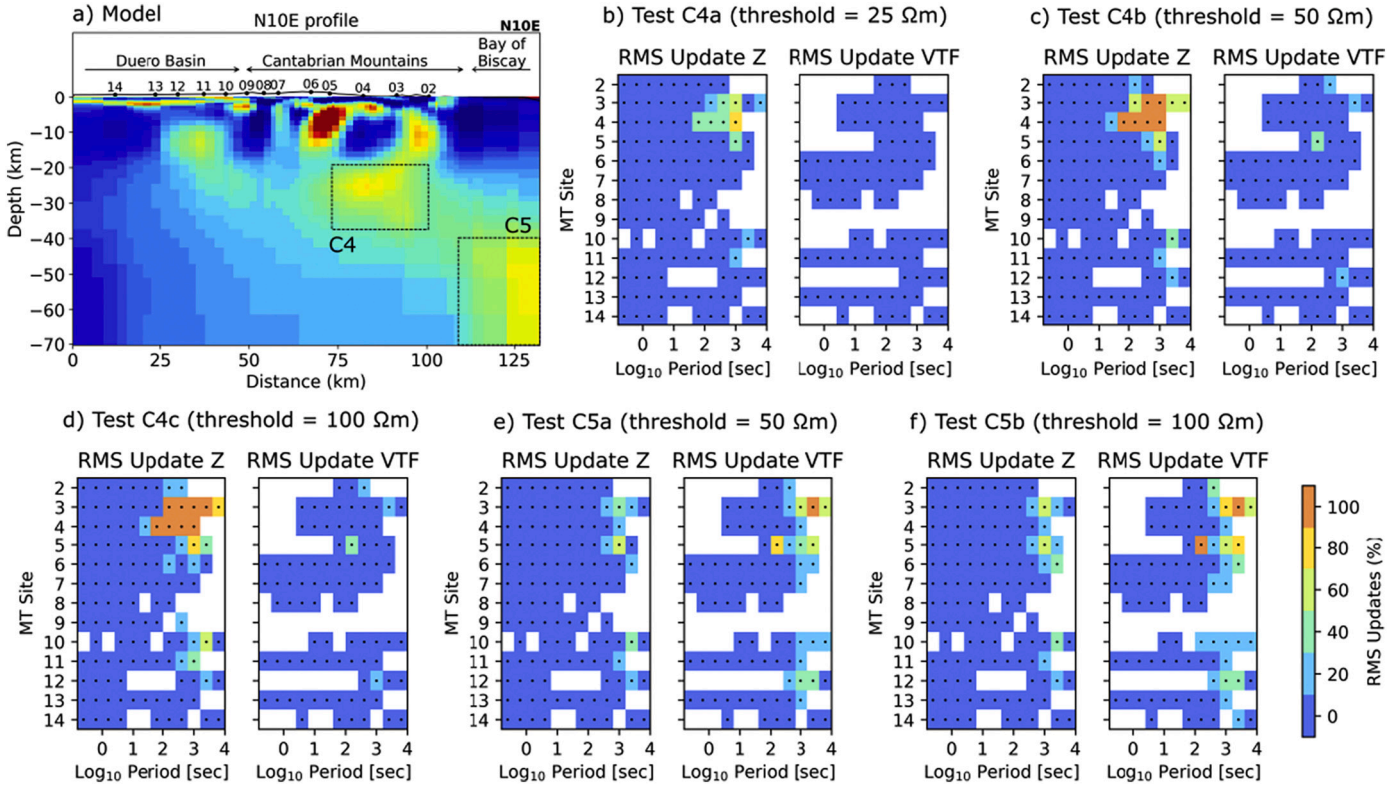

Fig. 8. Model assessment results for the different tests. The RMS updates are shown for both impedances and VTF, for each site as a function of frequency.

error floors, any difference in RMS points to misfits that are greater than the error floor. When the *RMS update* is presented as a function of frequency or data component it indicates which parts of the data are sensitive to the changes applied in the model.

We performed several tests independently, where in each case the resistivity of the feature of interest was substituted by a different resistivity value. Conductors C1, C2 and C3 were proved to be highly constrained by the data. We present here the sensitivity tests for the conductors C4 and C5. Fig. 8a shows the location of different perturbations that were applied to the final model and Fig. 8b-f shows the results of these tests. *RMS updates* $\leq$ 10% are represented in blue and indicate that the model perturbations have nearly no effects on the data. In contrast, we consider that *RMS updates* $>$ 10% are significant. An *RMS update* of 100% means that the misfit for a particular data point or group of points has doubled.

For the conductor C4 we tested an area comprised between 20 and 50 km depth where resistivities under a certain threshold value were raised to the threshold value. This conductor C4 has minimum resistivity values around 5 Ωm at 24 km depth. We performed 3 tests, C4a, C4b and C4c, using threshold values of 25 Ωm, 50 Ωm and 100 Ωm respectively. The results show all the perturbations affected the responses, in particular the impedance tensor for sites 03, 04 and 05 (directly located above the C4 anomaly) for periods greater than 100 s. Using a threshold of 25 Ωm (Fig. 8a) the effect on the responses is less pronounced (RMS updates between 25% and 75%) than for the tests using 50 Ωm and 100 Ωm (Fig. 8b and Fig. 8c, with RMS updates greater than 90%), but still significant. The VTF data seems relatively insensitive to these changes. These tests confirm that conductor C4 in its form is required by the data, with a maximum resistivity of ~25 Ωm in its center.

For conductor C5 we performed two tests using the same approach (Fig. 8a, Fig. 8d and Fig. 8e). In this case the area tested is comprised between depths of 40 km and 70 km and we used threshold values of 50 Ωm and 100 Ωm. These tests show that using a threshold value of 100 Ωm start to have a sensible effect on the data fit, affecting slightly the impedance at long period ($T > 500$ s) for sites 03 to 05 (*RMS update* $>$ 10%), and the VTF data for sites 03 and 05 at long periods. Thus, conductor C5 is not as well constrained as conductor C4. It is important to notice that the conductor C5 is located outside of the coverage of the MT sites, 15 km north of the survey, which makes it subject to ambiguity in terms of robustness. In any case, the location of this conductor in the continuation of the top of the dipping mantle, suggests a relation with it.

5. Interpretation and discussion

In this section we discuss the main features observed in the model, their correlation with existing interpretations and the tectonic implications. Fig. 9 shows the N10°E cross section of the 3-D inverse model, overlaid by a geological interpretation derived using geological data and existing crustal to lithospheric models, obtained from modeling of seismic, petrological and gravity data (Pedreira et al., 2015, Gallastegui et al., 2016).

The shallow elongated conductive zone C1 (values between 2 Ωm and 30 Ωm) is related to the Cenozoic sediments of the Duero foreland basin, deposited upon the highly resistive Paleozoic basement. Porous, permeable and water-saturated rocks are responsible for the high electrical conductivity of these formations. Sediment thickness inferred from the MT image varies, having a maximum thickness of 3500 m beneath site 13 and 2500 m beneath site 11. *El Campillo* exploration well, located between sites 12 and 11, reaches the basement at 2584 m below the surface (Lanaja, 1987). The largest sediment thickness beneath site 13 (Fig. 6d) is related to a local depocenter located in the footwall of a blind, north dipping Alpine thrust (El Campillo thrust), well imaged in oil exploration reflection profiles and ESCIN-2 deep seismic reflection profile (Pulgar et al., 1996, 1997; Gallastegui, 2000; Gallastegui et al., 2016).

The three elongated and north-dipping conductors (C2) located in

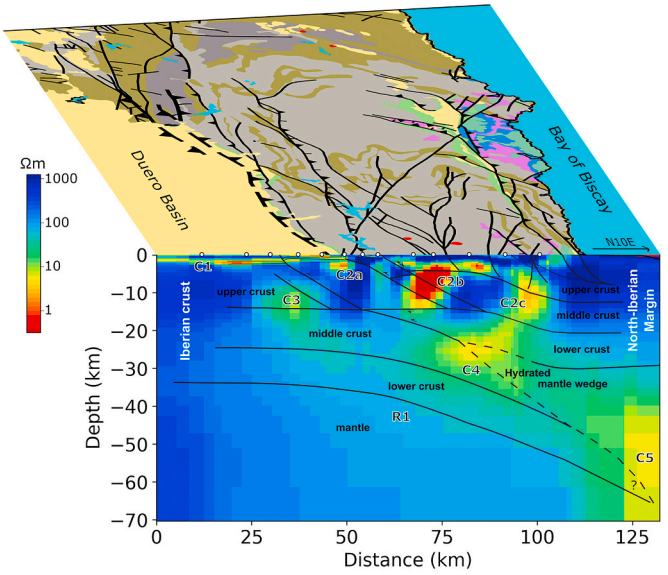

Fig. 9. N10°E oriented cross section across the 3-D model. The geological interpretation is based on the seismically constrained interpretations of Pedreira et al. (2015) and Gallastegui et al. (2016). See Fig. 1 for the legend of the geological map.

the upper crust of the Cantabrian Mountains correspond to fractured areas. These faults are either Alpine structures or Variscan/Late-Variscan structures, some of them reactivated during the Alpine Orogeny (Gallastegui et al., 2016). In either case, their conductive behavior is interpreted as fluids present in the fractured areas of the Paleozoic basement. Conductor C2a is related to the frontal thrust and marks the boundary between the Cenozoic sediments of the Duero basin to the south and the Paleozoic formations of the Cantabrian Mountains to the north. Conductor C2b is well marked and although it is manly oriented E-W, it has a NE-SW orientation west of the profile, and a NW-SE orientation east of the profile, which are the directions of the Late Variscan, subvertical faults in the area (Fig. 7). The spatial coincidence between the high conductive zone and the trace of these faults, as well as the great extent of the conductor both horizontally (Fig. 7) and vertically (reaching ~15 km depth, which is expected to be the base of the brittle crust) suggest that this anomaly is created by fluid circulation along several of these Late Variscan faults with different orientations, rather than by lithological heterogeneities. To the east, this conductor is associated with the continuation at depth of the Ruesga-Ubierna fault. The way these several conductors constituting conductor C2b are connected, both horizontally and vertically, is the preferred explanation for the phases exceeding 90 degrees. The conductor C2c is subvertical, reaching a depth of 15 km beneath the trace of the Cabuérniga normal fault. This long and deep structure shows at least 6 hydrothermal springs along its trace, with temperatures up to 65 °C (Heredia et al., 2022). We therefore also consider water circulation along this fault as the most plausible explanation for anomaly C2c. The geoelectrical signature of this fault reaches the detachment located at the top of the southwards indented Cantabrian Margin lower crust.

Conductor C3 is located approximately beneath the local depocenter observed in the Duero basin. In the ESCIN-2 seismic reflection profile, two parallel reflectors dipping northwards are located beneath the Duero basin, approximately in the same area, and are interpreted as blind basement thrusts, the northern one named as El Campillo thrust (Pulgar et al., 1996; Gallastegui et al., 2016). Both structures reach the Mesozoic layers at the base of the basin and extend downwards to the top of the middle crust, at 14 km depth (Gallastegui et al., 2016). East of the profile, the direction of the anomaly changes to ~NW-SE, which is the direction of the Late-Variscan faults, some of them reactivated

during the Alpine cycle (e.g. the Ubierna, Golobar and Rumaceo faults). The location of the C3 anomaly, its linear geometry and its orientation (Fig. 7) suggest that C3 is the conductive signature of these faults in the basement, the high conductivity being caused by the presence of fluids along the faults.

The conductive feature C4 is located between 20 and 30 km depth (Fig. 9), its southernmost extremity being located 30 km south of the coastline. The resistivities observed in the MT model are as low as 5 Ωm at 24 km depth and constrained by the sensitivity tests to be lower than 25 Ωm. A low velocity zone (Vp ~ 7.7 km/s), corresponding to the southernmost edge of the mantle wedge, was observed by the seismic refraction / wide angle reflection experiments (Marconi-1 profile, Ruiz et al., 2017) at a depth of ~28 km, 25 km south of the coastline. This low velocity zone is broadly coincident with the position of conductor C4, although the conductor is located a few kilometers shallower and southwards. Similar high conductivities in mantle wedges have been observed using magnetotellurics in several other locations worldwide (e.g. Worzewski et al., 2011; McGary et al., 2014), but rather correspond to hot and active subduction zones. In an active subduction zone context this type of anomaly is due to a water flux into the mantle wedge, resulting from the dehydration of the downgoing slab. In the Cantabrian Mountains, dehydration reactions in the subducting Iberian lower crust has been ruled out as the main water supplier into the mantle wedge, based on the estimated composition, pressure and temperature conditions at those depths (Pedreira et al., 2015). Pedreira et al. (2015) have suggested that the 1–2 wt% of water required to explain the low velocity anomalies in the mantle wedge would have its origin from an earlier percolation from the surface, which happened during the formation of the Cantabrian continental margin in the Mesozoic. The relative spatial correlation (Fig. 9) between the low velocity zone and the high conductivity anomaly supports the interpretation of a zone of hydrated mantle as the explanation for the high conductivity of C4. The amount of fluid deduced from the seismic velocities is enough to explain the low resistivities observed, according to the model of Reynard et al. (2011), considering a fluid with the salinity of seawater. The presence of anomaly C4 in that position is roughly compatible with the crustal models presented by Gallastegui (2000), Pedreira et al. (2015) and Teixell et al. (2018), but it is more difficult to explain with the model presented by García-Senz et al. (2020). Although their model for the "Polientes section" lies ~40–50 km to the east, they propose that the Moho is at >40 km depth beneath the trace of the Cabuérniga Fault and only shallows from the position of the MT station 2 to the north, with a large body of exhumed mantle rising to 14 km depth approximately beneath the coastline. Even considering that the structure might change abruptly from the Polientes section to the section studied here, we must note that the presence of such a feature, which would likely have a conductive response as a result of its serpentinization, would be incompatible with the orientation of the induction arrows of the northern stations (Fig. 2a).

The conductor C5, located between ~40 km and more than 70 km depth in the northern margin of the model correlates with the prolongation of the subducting Iberian lower crust to the north beneath the Bay of Biscay. This spatial coincidence suggests a relation with the crustal root. However, with the current data and the lack of resolution for its conductivity values and precise localization, it is difficult to interpret it in an unambiguous way. According to the petrological/geophysical modeling of the subducting Iberian crust (Pedreira et al., 2015), water released by eclogitization reactions are only expected in very small amounts if the crustal root reaches more than 60 km depth. The possibility of such a deep root cannot be ruled out according to the available geophysical data, and can be perfectly compatible with isostatic equilibrium, although a shallower root (~60 km depth) seems to explain the seismic tomography data slightly better (Pedreira et al., 2015). With a shallower crustal root (~60 km), the estimated pressure/temperature conditions are such that the solidus curve for the subducting lower crustal are just reached (Pedreira et al., 2015). Due to the uncertainties in these determinations, including the composition of the subducting lower crust, we consider likely that small amounts of water or melt could possibly be released in the deep crustal root, potentially creating a zone of lower resistivities. This crustal root continues to the east up to the Pyrenees (Pedreira et al., 2007), where other authors also related high conductivities to partial melting of the subducted Iberian lower crust (Pous et al., 1995a, 1995b; Ledo et al., 2000; Partzsch et al., 2000; Campanyà et al., 2011).

6. Conclusions

Thirteen magnetotelluric soundings with broad-band and long period instruments were acquired along an N-S profile crossing the Cantabrian Mountains and the Duero basin. The 3-D nature of the MT data in this area was determined from the analysis of the MT impedance and phase tensors. In order to perform a 3-D inversion of this dataset along an N-S profile we adopted a specific inversion workflow. Ultimately, the 3-D resistivity model was obtained by the 3-D joint inversion of the full impedance tensor and the magnetic transfer functions. This workflow resulted in a 3-D model with minimal off-profile structures, which agrees with our prior knowledge of a regional *E*-W oriented subduction system with local complex tectonics in the upper crust of the Cantabrian Mountains. The correlation between the geoelectric image, the existing geophysical models and the surface geology provides a deeper understanding of the lithospheric processes. The Duero basin sediments are clearly imaged and are consistent with well log and seismic reflection data. Conductive north dipping to subvertical zones in the Paleozoic basement are related to enhanced permeability along the main Alpine and reactivated Variscan and Late-Variscan faults. Main faults in the Cantabrian Mountains were detected as conductors concentrated in the upper crust. They do not reach more than 10 km in the southern part of the Cantabrian Mountains and 15 km in the northern part. A deep conductive zone was detected above the northward subducting slab of the Iberian crust just at the top of the mantle wedge, attributed to hydration of the upper mantle during the Mesozoic formation of the North-Iberian continental margin. Finally, in the northern part of the model a deep conductor at greater depth (from ~40 to more than 70 km) was detected. This conductor was poorly constrained and new data recorded offshore further north of the profile is required to confirm its presence. We tentatively propose that very small amounts of water or partial melt released in the subducting Iberian crust, as proposed further east in the Pyrenees, might be the cause of that high conductivity.

CRediT authorship contribution statement

Hoël Seillé: Conceptualization, Methodology, Software, Writing – original draft, Writing – review & editing. **Jaume Pous:** Supervision, Conceptualization, Methodology, Software, Writing – review & editing. **David Pedreira:** Visualization, Writing – original draft, Writing – review & editing. **Jorge Gallastegui:** Writing – review & editing. **Ivan Romero-Ruiz:** Software, Formal analysis. **Javier A. Pulgar:** Writing – review & editing.

Declaration of Competing Interest

The authors declare that they have no known competing financial interests or personal relationships that could have appeared to influence the work reported in this paper.

Acknowledgments

We thank two anonymous reviewers for their constructive comments. This research was funded by the Spanish Ministry of Education and Science through the Consolider-Ingenio 2010 Project TOPO-IBERIA (CSD2006-09727). This is a contribution of the GEOTEC Group, with

additional funding from the European Regional Development Funds and the Government of the Principality of Asturias (IDI/2018/000216). Fig. 2b was produced using the open-source Python module MTPy (Krieger and Peacock, 2014; Kirkby et al., 2019).

Appendix A. Supplementary data

Supplementary data to this article can be found online at https://doi.org/10.1016/j.tecto.2022.229310.

References

Alonso, J.L., Pulgar, J.A., García-Ramos, J.C., Barba, P., 1996. Tertiary basins and Alpine tectonics in the Cantabrian Mountains (NW Spain). In: Tertiary Basins of Spain. https://doi.org/10.1017/cbo9780511524851.031.

Amante, C., Eakins, B.W., 2009. ETOPO1 1 Arc-minute global relief model: procedures, data sources and analysis. In: NOAA Technical Memorandum NESDIS NGDC-24. https://doi.org/10.1594/PANGAEA.769615.

Anahnah, F., Galindo-Zaldívar, J., Chalouan, A., Pous, J., Ruano, P., Pedrera, A., Asensio, E., 2011. Crustal resistivity structure of the southwestern transect of the Rif Cordillera (Morocco). Geochem. Geophys. Geosyst. 12 (12) https://doi.org/10.1029/2011GC003783 n/a-n/a.

Bahr, K., 1988. Interpretation of the magnetotelluric impedance tensor: regional induction and local telluric distortion. Journal of geophysics 62 (1), 119–127.

Barnolas, A., Pujalte, V., 2004. La cordillera pirenaica. In: Vera, J.A. (Ed.), Geología de España. IGME-SGE, pp. 233–343.

Bastida, F., Blanco-Ferrera, S., García-López, S., Sanz-López, J., Valín, M.L., 2004. Transition from diagenesis to metamorphism in a calcareous tectonic unit of the Iberian Variscan belt (central massif of the Picos de Europa, NW Spain). Geol. Mag. https://doi.org/10.1017/S0016756804009653.

Berdichevsky, M.N., Dmitriev, V.I., Golubtsova, N.S., Mershchikova, N.A., Pushkarev, P. Y., 2003. Magnetovariational sounding: new possibilities. Izvestiya Phys. Solid Earth 39 (9), 701–727.

Brasse, H., Schäfer, A., Díaz, D., Alvarado, G.E., Muñoz, A., Mütschard, L., 2015. Deep-crustal magma reservoirs beneath the Nicaraguan volcanic arc, revealed by 2-D and semi 3-D inversion of magnetotelluric data. Phys. Earth Planet. Inter. https://doi.org/10.1016/j.pepi.2015.08.004.

Bullard, E.C., 1965. Fit of the continents around the Atlantic. Science. https://doi.org/10.1126/science.148.3670.664.

Cadenas, P., Fernández-Viejo, G., Pulgar, J.A., Tugend, J., Manatschal, G., Minshull, T.A., 2018. Constraints Imposed by Rift Inheritance on the Compressional Reactivation of a Hyperextended margin: Mapping Rift Domains in the North Iberian margin and in the Cantabrian Mountains. Tectonics. https://doi.org/10.1002/2016TC004454.

Caldwell, T.G., Bibby, H.M., Brown, C., 2004. The magnetotelluric phase tensor. Geophys. J. Int. 158 (2), 457–469. https://doi.org/10.1111/j.1365-246X.2004.02281.x.

Campanyà, J., Ledo, J., Queralt, P., Marcuello, A., Liesa, M., Muñoz, J.A., 2011. Lithospheric characterization of the Central Pyrenees based on new magnetotelluric data. Terra Nova. https://doi.org/10.1111/j.1365-3121.2011.01001.x.

Chave, A.D., Jones, A.G., 2012. The magnetotelluric method: theory and practice. In: The Magnetotelluric Method: Theory and Practice. https://doi.org/10.1017/CBO9781139020138.

Chave, A.D., Thomson, D.J., Ander, M.E., 1987. On the robust estimation of power spectra, coherences and transfer functions. J. Geophys. Res. 92 (B1), 633–648. https://doi.org/10.1029/JB092iB01p00633.

DeFelipe, I., Pedreira, D., Pulgar, J.A., Iriarte, E., Mendia, M., 2017. Mantle exhumation and metamorphism in the Basque-Cantabrian Basin (N Spain). Stable and clumped isotope analysis in carbonates and comparison with ophicalcites in the North-Pyrenean Zone (Urdach and Lherz). Geochem. Geophys. Geosyst. 18 https://doi.org/10.1002/2016GC006690.

DeFelipe, I., Pulgar, J.A., Pedreira, D., 2018. Crustal structure of the eastern Basque-Cantabrian zone – Western Pyrenees: from the cretaceous hyperextension to the Cenozoic inversion. Rev. Soc. Geol. Esp. 31 (2), 69–82. https://doi.org/10.13039/501100003329.

Evans, R.L., 2012. Chapter 3: Earth's electromagnetic environment. Part 1: conductivity of earth materials. In: Chave, A.D., Jones, A.G. (Eds.), The Magnetotelluric Method: Theory and Practice. Cambridge Univ. Press, Cambridge, U. K.

Evans, R.L., Wannamaker, P.E., McGary, R.S., Elsenbeck, J., 2014. Electrical structure of the Central Cascadia subduction zone: the EMSLAB Lincoln Line revisited. Earth Planet. Sci. Lett. https://doi.org/10.1016/j.epsl.2013.04.021.

Fernández Viejo, G., 1997. Estructura cortical de la Cordillera Cantábrica y su transición a la Cuenca del Duero a partir de datos de sísmica de refracción/reflexión de gran ángulo. Unpublished PhD Thesis. Universidad de Barcelona, España, 309 pp.

Fernández-Viejo, G., Gallart, J., Pulgar, J.A., Gallastegui, J., Dañobeitia, J.J., Córdoba, D., 1998. Crustal transition between continental and oceanic domains along the North Iberian margin from wide angle seismic and gravity data. Geophys. Res. Lett. https://doi.org/10.1029/1998gl900149.

Fernández-Viejo, G., Gallart, J., Pulgar, J.A., Córdoba, D., Dañobeitia, J.J., 2000. Seismic signature of Variscan and Alpine tectonics in NW Iberia: Crustal structure of the Cantabrian Mountains and Duero basin. J. Geophys. Res. Solid Earth. https://doi.org/10.1029/1999jb900321.

Fernández-Viejo, G., Cadenas, P., Acevedo, J., Llana-Fúnez, S., 2021. The unevenness of the north Iberian crustal root, a snapshot of an elusive stage in margin reactivation. Geology 49, 1426–1430.

Fillon, C., Pedreira, D., Van Der Beek, P.A., Huismans, R.S., Barbero, L., Pulgar, J.A., 2016. Alpine exhumation of the central Cantabrian Mountains, Northwest Spain. Tectonics. https://doi.org/10.1002/2015TC004050.

Gallart, J., Fernández-Viejo, G., Díaz, J., Vidal, N., Pulgar, J.A., 1997. Deep structure of the transition between the Cantabrian Mountains and the North Iberian Margin from Wide-Angle ESCI-N data. Rev. Soc. Geol. Esp. 8 (4), 365–382.

Gallart, J. Azor, Fernández, M., Pulgar, J.A., 2015. Iberia geodynamics: an integrative approach from the Topo-Iberia framework. Tectonophysics. https://doi.org/10.1016/j.tecto.2015.09.010.

Gallastegui, J., 2000. Estructura cortical de la cordillera y margen continental cantábricos: perfiles ESCI-N. In: Trabajos de Geología, vol. 22. Universidad de Oviedo, España, 220 pp.

Gallastegui, J., Pulgar, J.A., Gallart, J., 2002. Initiation of an active margin at the North Iberian continent-ocean transition. Tectonics. https://doi.org/10.1029/2001TC901046.

Gallastegui, J., Pulgar, J.A., Gallart, J., 2016. Alpine tectonic wedging and crustal delamination in the Cantabrian Mountains (NW Spain). Solid Earth 7, 1043–1057. https://doi.org/10.5194/se-7-1043-2016.

Garcia, X., Seillé, H., Elsenbeck, J., Evans, R.L., Jegen, M., Hölz, S., Ranero, C.R., 2015. Structure of the mantle beneath the Alboran Basin from magnetotelluric soundings. Geochem. Geophys. Geosyst. 16 (12), 4261–4274. https://doi.org/10.1002/2015GC006100.

García-Senz, J., Pedrera, A., Ayala, C., Ruiz-Constán, A., Robador, A., Rodríguez-Fernández, L.R., 2020. Inversion of the north Iberian hyperextended margin: the role of exhumed mantle indentation during continental collision. Geol. Soc. Lond. Spec. Publ. 490, 177–198.

Gasparrini, M., Bechstädt, T., Boni, M., 2006. Massive hydrothermal dolomites in the southwestern Cantabrian Zone (Spain) and their relation to the late Variscan evolution. Mar. Pet. Geol. https://doi.org/10.1016/j.marpetgeo.2006.05.003.

Groom, R.W., Bailey, R.C., 1989. Decomposition of magnetotelluric impedance tensors in the presence of local three-dimensional galvanic distortion. J. Geophys. Res. 94 (B2), 1913–1925. https://doi.org/10.1029/JB094iB02p01913.

Heise, W., Pous, J., 2003. Anomalous phases exceeding 90° in magnetotellurics: anisotropic model studies and a field example. In. Geophys. J. Int. 155. Retrieved from. https://academic.oup.com/gji/article-abstract/155/1/308/714207.

Heise, W., Ogawa, Y., Bertrand, E.A., Caldwell, T.G., Yoshimura, R., Ichihara, H., Kinoshita, Y., 2019. Electrical resistivity imaging of the inter-plate coupling transition at the Hikurangi subduction margin, New Zealand. Earth Planet. Sci. Lett. 524, 115710 https://doi.org/10.1016/j.epsl.2019.115710.

Heredia, N., Gómez, J.A., Molinero, R., León, C., Pineda, A., Delgado, B., Varea, R., Pulgar, J.A., Navas, M., 2010. Selección y caracterización de áreas y estructuras con capacidad de almacenamiento geológico de CO2 en España, Vol I-1: Cadena Cantábrica y Cuenca del Duero (Geología). In: Fondo Documental del IGME (SID Code: 64044), 113 pp. (Unpublished).

Heredia, N., Martín-González, F., Farias, P., García- Sansegundo, J., Pedreira, D., Gonzalo-Guerra, B., García-Davia, G., Mateos, G., Flórez-Rodríguez, A.G., 2022. Geology of the Cabuérniga Fault System: evolution of a large Alpine structure with Variscan inheritance. J. Maps. https://doi.org/10.1080/17445647.2021.2010612.

Ichihara, H., Mogi, T., 2009. A realistic 3-D resistivity model explaining anomalous large magnetotelluric phases: the L-shaped conductor model. Geophys. J. Int. https://doi.org/10.1111/j.1365-246X.2009.04310.x.

Jammes, S., Manatschal, G., Lavier, L., Masini, E., 2009. Tectonosedimentary evolution related to extreme crustal thinning ahead of a propagating ocean: example of the western Pyrenees. Tectonics. https://doi.org/10.1029/2008TC002406.

Kirkby, A., Zhang, F., Peacock, J., Hassan, R., Duan, J., 2019. The MTPy software package for magnetotelluric data analysis and visualisation. J. Open Source Softw. 4 (37), 1358. https://doi.org/10.21105/joss.01358.

Krieger, L., Peacock, J.R., 2014. MTpy: a Python toolbox for magnetotellurics. Comput. Geosci. 72, 167–175. https://doi.org/10.1016/j.cageo.2014.07.013.

Lagabrielle, Y., Labaume, P., De Saint Blanquat, M., 2010. Mantle exhumation, crustal denudation, and gravity tectonics during cretaceous rifting in the Pyrenean realm (SW Europe): Insights from the geological setting of the lherzolite bodies. Tectonics. https://doi.org/10.1029/2009TC002588.

Lanaja, J.M., 1987. Contribución de la exploración petrolífera al conocimiento de la geología de España. ITGE, Madrid, 465 pp.

Ledo, J., Ayala, C., Pous, J., Queralt, P., Marcuello, A., Muñoz, J.A., 2000. New geophysical constraints on the deep structure of the Pyrenees. Geophys. Res. Lett. https://doi.org/10.1029/1999GL011005.

Lepvrier, C., Martínez-García, E., 1990. Fault development and stress evolution of the post-Hercynian Asturian Basin (Asturias and Cantabria, northwestern Spain). Tectonophysics. https://doi.org/10.1016/0040-1951(90)90447-G.

Lezaeta, P., Haak, V., 2003. Beyond magnetotelluric decomposition: Induction, current channeling, and magnetotelluric phases over 90°. J. Geophys. Res. Solid Earth 108 (B6). https://doi.org/10.1029/2001jb000990.

López-Gómez, J., Martín-González, F., Heredia, N., de la Horra, R., Barrenechea, J.F., Cadenas, P., Juncal, M., Diez, J.B., Borruel-Abadía, V., Pedreira, D., García-Sansegundo, J., Farias, P., Galé, C., Lago, M., Ubide, T., Fernández-Viejo, G., Gand, G., 2019. New lithostratigraphy for the Cantabrian Mountains: A common tectonostratigraphic evolution for the onset of the Alpine cycle in the W Pyrenean realm, N Spain. Earth Sci. Rev. 188, 249–271. https://doi.org/10.1016/j.earscirev.2018.11.008.

Macchiavelli, C., Vergés, J., Schettino, A., Fernàndez, M., Turco, E., Casciello, E., Tunini, L., 2017. A New Southern North Atlantic Isochron Map: insights into the drift

of the Iberian Plate since the late cretaceous. J. Geophys. Res. Solid Earth. https://doi.org/10.1002/2017JB014769.
Martín-González, F., Heredia, N., 2011. Complex tectonic and tectonostratigraphic evolution of an Alpine foreland basin: the western Duero Basin and the related Tertiary depressions of the NW Iberian Peninsula. Tectonophysics. https://doi.org/10.1016/j.tecto.2010.03.002.
Matsuno, T., Seama, N., Evans, R.L., Chave, A.D., Baba, K., White, A., Utada, H., 2010. Upper mantle electrical resistivity structure beneath the central Mariana subduction system. Geochem. Geophys. Geosyst. 11 (9), Q09003. https://doi.org/10.1029/2010GC003101.
McGary, R.S., Evans, R.L., Wannamaker, P.E., Elsenbeck, J., Rondenay, S., 2014. Pathway from subducting slab to surface for melt and fluids beneath Mount Rainier. Nature. https://doi.org/10.1038/nature13493.
McNeice, G.W., Jones, A.G., 2001. Multisite, multifrequency tensor decomposition of magnetotelluric data. Geophysics 66 (1), 158–173. https://doi.org/10.1190/1.1444891.
Nirrengarten, M., Manatschal, G., Tugend, J., Kusznir, N., Sauter, D., 2018. Kinematic Evolution of the Southern North Atlantic: Implications for the Formation of Hyperextended Rift Systems. Tectonics. https://doi.org/10.1002/2017TC004495.
Partzsch, G.M., Schilling, F.R., Arndt, J., 2000. The influence of partial melting on the electrical behavior of the crustal rocks: laboratory examinations, model calculations and the geological interpretations. Tectonophysics 317, 189–203.
Patro, P.K., Egbert, G.D., 2011. Application of 3D inversion to magnetotelluric profile data from the Deccan Volcanic Province of Western India. Phys. Earth Planet. Inter. 187 (1–2), 33–46. https://doi.org/10.1016/j.pepi.2011.04.005.
Pedreira, D., Pulgar, J.A., Gallart, J., Díaz, J., 2003. Seismic evidence of Alpine crustal thickening and wedging from the western Pyrenees to the Cantabrian Mountains (North Iberia). J. Geophys. Res. Solid Earth 108 (B4). https://doi.org/10.1029/2001jb001667.
Pedreira, D., Pulgar, J.A., Gallart, J., Torné, M., 2007. Three-dimensional gravity and magnetic modeling of crustal indentation and wedging in the western Pyrenees-Cantabrian Mountains. J. Geophys. Res. Solid Earth. https://doi.org/10.1029/2007JB005021.
Pedreira, D., Afonso, J.C., Pulgar, J.A., Gallastegui, J., Carballo, A., Fernández, M., García-Moreno, O., 2015. Geophysical-petrological modeling of the lithosphere beneath the Cantabrian Mountains and the North-Iberian margin: geodynamic implications. Lithos. https://doi.org/10.1016/j.lithos.2015.04.018.
Pérez-Estaún, A., Martínez-Catalán, J.R., Bastida, F., 1991. Crustal thickening and deformation sequence in the footwall to the suture of the Variscan belt of Northwest Spain. Tectonophysics. https://doi.org/10.1016/0040-1951(91)90060-6.
Pous, J., Ledo, J., Marcuello, A., Daignières, M., 1995a. Electrical resistivity model of the crust and upper mantle from a magnetotelluric survey through the Central Pyrenees. Geophys. J. Int. 121 (3), 750–762.
Pous, J., Munoz, J.A., Ledo, J.J., Liesa, M., 1995b. Partial melting of subducted continental lower crust in the Pyrenees. J. Geol. Soc. Lond. https://doi.org/10.1144/gsjgs.152.2.0217.
Pous, J., Queralt, P., Marcuello, A., 2001. Magnetotelluric signature of the western Cantabrian Mountains. Geophys. Res. Lett. https://doi.org/10.1029/2000GL011915.
Pous, J., Martínez Poyatos, D., Heise, W., Santos, F.M., Galindo-Zaldívar, J., Ibarra, P., Pedrera, A., Ruiz-Constán, A., Anahnah, F., Gonçalves, R., Mateus, A., 2011. Constraints on the crustal structure of the internal Variscan Belt in SW Europe: A magnetotelluric transect along the eastern part of Central Iberian Zone, Iberian Massif. J. Geophys. Res. Solid Earth 116 (B2).
Pous, J., Muñoz-Martín, A., Olaiz, A.J., Seillé, H., de Vicente, G., 2012. Analisis de la estructura alpina de la corteza del centro de la Peninsula Iberica: Una seccion Magneto-Telurica a traves del Sistema Central (Sierra de Gredos). Geo-Temas 13 (4–8), 2012.
Pulgar, J.A., Gallart, J., Fernández-Viejo, G., Perez-Estaún, A., Álvarez-Marrón, J., ESCIN group, 1996. Seismic image of the Cantabrian Mountains in the western extension of the Pyrenees from integrated ESCIN reflection and refraction data. Tectonophysics. https://doi.org/10.1016/S0040-1951(96)00114-X.
Pulgar, J.A., Pérez-Estaún, A., Gallart, J., Alvarez-Marrón, J., Gallastegui, J., Alonso, J.L., Group, E, 1997. The ESCI-N2 deep seismic reflection profile: a traverse across the Cantabrian Mountains and adjacent Duero basin. Rev. Soc. Geol. Esp. 8 (4), 383–394.
Quintana, L., Pulgar, J.A., Alonso, J.L., 2015. Displacement transfer from borders to interior of a plate: A crustal transect of Iberia. Tectonophysics. https://doi.org/10.1016/j.tecto.2015.08.046.
Rat, P., 1988. The Basque-Cantabrian basin between the Iberian and European plates: some facts but still many problems. Rev. Soc. Geol. Esp. 1 (3–4), 327–348.
Reynard, B., Mibe, K., Van de Moortèle, B., 2011. Electrical conductivity of the serpentinised mantle and fluid flow in subduction zones. Earth Planet. Sci. Lett. 307, 387–394. https://doi.org/10.1016/j.epsl.2011.05.013.
Roca, E., Muñoz, J.A., Ferrer, O., Ellouz, N., 2011. The role of the Bay of Biscay Mesozoic extensional structure in the configuration of the Pyrenean orogen: Constraints from the MARCONI deep seismic reflection survey. Tectonics. https://doi.org/10.1029/2010TC002735.
Rodríguez Fernández, L.R., Pedrera, A., Pous, J., Ayala, C., González Menéndez, L., Ibarra, P., Seillé, H., 2015. Crustal structure of the south-western termination of the Alpine Pyrenean-Cantabrian Orogen (NW Iberian Peninsula). Tectonophysics. https://doi.org/10.1016/j.tecto.2015.06.010.
Rosenbaum, G., Lister, G.S., Duboz, C., 2002. Relative motions of Africa, Iberia and Europe during Alpine orogeny, Tectonophysics. https://doi.org/10.1016/S0040-1951(02)00442-0.
Ruiz, M., Díaz, J., Pedreira, D., Gallart, J., Pulgar, J.A., 2017. Crustal structure of the North Iberian continental margin from seismic refraction/wide-angle reflection profiles. Tectonophysics. https://doi.org/10.1016/j.tecto.2017.07.008.
Seillé, H., Salas, R., Pous, J., Guimerà, J., Gallart, J., Torné, M., Mas, R., 2015. Crustal structure of an intraplate thrust belt: the Iberian Chain revealed by wide-angle seismic, magnetotelluric soundings and gravity data. Tectonophysics. https://doi.org/10.1016/j.tecto.2015.08.027.
Siripunvaraporn, W., Egbert, G., 2009. WSINV3DMT: Vertical magnetic field transfer function inversion and parallel implementation. Phys. Earth Planet. Inter. 173 (3–4), 317–329. https://doi.org/10.1016/j.pepi.2009.01.013.
Siripunvaraporn, W., Egbert, G., Uyeshima, M., 2005. Interpretation of two-dimensional magnetotelluric profile data with three-dimensional inversion: synthetic examples. Geophys. J. Int. 160 (3), 804–814. https://doi.org/10.1111/j.1365-246X.2005.02527.x.
Srivastava, S.P., Sibuet, J.C., Cande, S., Roest, W.R., Reid, I.D., 2000. Magnetic evidence for slow seafloor spreading during the formation of the Newfoundland and Iberian margins. Earth Planet. Sci. Lett. https://doi.org/10.1016/S0012-821X(00)00231-4.
Teixell, A, 1998. Crustal structure and orogenic material budget in the west central Pyrenees. Tectonics 17 (3), 395–406.
Teixell, A., Labaume, P., Ayarza, P., Espurt, N., de Saint Blanquat, M., Lagabrielle, Y., 2018. Crustal structure and evolution of the Pyrenean-Cantabrian belt: A review and new interpretations from recent concepts and data. Tectonophysics. https://doi.org/10.1016/j.tecto.2018.01.009.
Varentsov, I.M., 2006. Chapter 10 Arrays of simultaneous electromagnetic soundings: design, data processing and analysis. In: Methods in Geochemistry and Geophysics. https://doi.org/10.1016/S0076-6895(06)40010-X.
Vergés, J., García-Senz, J., 2001. Mesozoic evolution and Cainozoic inversion of the Pyrenean rift. Mém. Du Muséum Natl. d'histoire Nat. 1993 (186), 187–212.
van der Voo, R., 1969. Paleomagnetic evidence for the rotation of the Iberian Peninsula. Tectonophysics. https://doi.org/10.1016/0040-1951(69)90063-8.
Weckmann, U., Ritter, O., Haak, V., 2003a. A magnetotelluric study of the Damara Belt in Namibia 2. MT phases over 90° reveal the internal structure of the Waterberg Fault/Omaruru Lineament. Phys. Earth Planet. Inter. 138 (2), 91–112. https://doi.org/10.1016/S0031-9201(03)00079-7.
Weckmann, U., Ritter, O., Haak, V., 2003b. Images of the magnetotelluric apparent resistivity tensor. In. Geophys. J. Int. 155. Retrieved from. https://academic.oup.com/gji/article-abstract/155/2/456/597370.
Worzewski, T., Jegen, M., Kopp, H., Brasse, H., Taylor Castillo, W., 2011. Magnetotelluric image of the fluid cycle in the Costa Rican subduction zone. Nat. Geosci. https://doi.org/10.1038/ngeo1041.